LAWRENCE
LIVERMORE
NATIONAL
LABORATORY

LLNL-TR-665701

Spallation As The Dominant Source of Pusher-Fuel and Hot-Spot Mix In ICF Capsules

C. D. Orth

December 29, 2014

Disclaimer

This work performed under the auspices of the U.S. Department of Energy by Lawrence Livermore National Laboratory under Contract DE-AC52-07NA27344.

Spallation As The Dominant Source of Pusher-Fuel and Hot-Spot Mix In ICF Capsules

By Charles D. Orth, PhD

Abstract

We report that the dominant source of pusher-fuel and hot-spot "mix" that has degraded the yields of modern ICF capsules designed and fielded to achieve high yield has likely been the spallation of small chunks or "grains" of pusher material into the fuel regions—not hydrodynamic instabilities. Such "spallation mix" occurs at the passage of the first strong shock whenever (1) the solid pusher adjacent to the fuel changes its phase by nucleation, and (2) such material when shocked (i.e., compressed and superheated, but still a solid) is subject to spallation when suddenly decompressed. When such spallation occurs, we show that it is the dominant mix mechanism by comparing the predictions of a spallation-mix model with measured experimental data, and by referring to direct experimental observations. We also explain how to eliminate this mix mechanism and thus allow higher yields for ICF capsules.

Introduction

Experimental yields from inertial confinement fusion (ICF) capsules fielded in laboratories prior to 2013 have typically been a factor of ten or more lower than expected from 1D or 2D computer calculations. Investigators have therefore worked diligently for decades trying to explain how hydrodynamic instabilities might cause such low yields. More recent experiments [1-4] have been a bit more consistent with computer simulations, but the reasons advanced for the improved performance and the changes in target design suggested for future improvements don't take into account what we report here as the most likely mechanism that degrades capsule yield. We therefore describe the physics of this uninvestigated mechanism in this paper, and explain why this mechanism is typically the dominant mechanism for the degradation of ICF capsule yields.

There are of course many possible target imperfections and physical mechanisms that might degrade the performance of ICF targets, including the following (where the term "pusher" refers to the capsule layer next to the fuel, whether or not it is also the outermost "ablator" layer):

- Ablator and/or pusher surface-finish or bulk-density irregularities that cause either (1) hydrodynamic instabilities at the ablation front in the ablator due to differential responses to uniform drive pressures, or (2) Rayleigh-Taylor (RT) instabilities at the pusher-fuel interface that grow upon pusher deceleration just before maximum fuel compression,
- Richtmyer-Meshkov (RM) instabilities along the pusher-fuel interface resulting from the passage of a shock wave,
- Asymmetries in the X-ray (or direct) drive that cause severe non-roundness of the imploded fuel regions,
- Initial "imprinting" of non-uniformities upon the ablator caused by drive irradiation (e.g., 3ω laser light) that did not fully convert to X-rays upon interacting with hohlraum walls.
- Structures holding the capsule in a hohlraum (e.g., plastic "tents") that "imprint" irregularities on the pusher-fuel interface,
- Fuel fill tubes that cause perturbations in the pusher-fuel interface, and
- Cryogenic fuel shell-thickness non-uniformities or fuel surface irregularities.

Great care has therefore been taken to avoid these potential sources of degradation, and in particular, to have surface finishes of (e.g.) < 20 nm RMS for modes > 30. Even so, experimental yields have generally been significantly degraded from what is desired. In most cases, investigators have suspected that some of the pusher material has somehow penetrated the deuterium-tritium (DT) fuel regions and degraded the burn, so the general subject is labeled a "mix" issue (i.e., a "mix" of pusher material into the DT fuel and/or hot spot). The conundrum has been that none of the above mechanisms can adequately explain the mix thought to be required, at least not without a great deal of conjecture.

We report here that the primary reason for this conundrum is that the dominant mix mechanism is not being considered in the target-design codes nor in the post-experiment analyses. This dominant source of mix is "spallation mix," which is caused by spallation of small chunks or "grains" of the pusher material into the fuel regions (i.e., into the cryogenic or gaseous fuel and/or central DT hot spot). As we will describe in this paper, such spallation occurs at the passage of the first strong shock whenever (1) the solid pusher adjacent to the fuel changes its phase by nucleation, and (2) such material when shocked (i.e., compressed and superheated, but still a solid) is subject to spallation when suddenly decompressed. The physics of phase nucleation is not in current target-design codes.

Although investigators have concentrated on RT and other instabilities to try to explain the mix, we concluded in 1985 that spallation mix is typically the dominant mix mechanism because it creates chunks of pusher material that can penetrate the fuel regions *much farther* than any spikes or other perturbations arising from RT instabilities. Recent information regarding how materials change phase supports our earlier conclusions, as we explain in a subsequent Section of this paper. We therefore describe our spallation-mix model here and show that its predictions agree remarkably well with measured ICF hohlraum data. Such success should be helpful to those fielding capsule experiments at the National Ignition Facility (NIF).

Specifically, we encourage code developers to (1) incorporate the physics of spallation mix into all computer codes that are used to calculate expected neutron yields from ICF capsules, or at least (2) be aware of this physics and how it can modify target performance. As we will show, the mere awareness of the physics of spallation mix allows one to understand how target design can be modified to avoid such mix, thus permitting higher ICF yields. Elimination of spallation mix may thus allow "ignition" to be achieved at the NIF.

We emphasize that RT and other mix mechanisms may well contribute to a capsule's yield degradation, because such mechanisms can indeed degrade performance for certain conditions. However, under the typical fielding conditions for modern ICF capsules with smooth surface finishes and relatively smooth drive irradiations, spallation mix is usually the dominant mix mechanism because (1) the materials used to contain the DT fuel tend to spall under shock loading and sudden decompression, (2) target designers try to minimize the preheat of the pusher and fuel so their compression occurs along the lowest-possible adiabats, (3) spallation mix, when it occurs, can penetrate *much farther* into the fuel regions than RT or other instabilities (which is evident based on just the g/cm^2 of the spalled pusher chunks penetrating the DT), and (4) RT instabilities need not be significant (by themselves) for capsules with smooth surface finishes and smooth drive irradiations. As we will show, item (2) is not the most effective approach if item (1) permits spallation mix to be the dominant mix mechanism. A more effective approach in such a case is to tailor the temporal drive profile and select capsule materials and drive wavelengths so that spallation mix is minimized or completely eliminated.

The Inherent Physics of Spallation Mix

The physics that is missing in current target design codes is the physics of spallation arising from the passage of a shock through a pusher whose phase changes by nucleation. Nucleation of a phase change is a well-known phenomenon [5] that is *inherent* whenever collective effects are involved in the phase change (as for, e.g., a metal) as opposed to local effects (as for, e.g., silicon). For example, a metal having band gaps can be superheated well above its normal liquefaction temperature but not change from a solid to a liquid and instead remain in a metastable state until the energetics in small regions of the material permit a phase change that is then able to propagate to surrounding superheated material. There are two critical requirements for the metastable state to change to the normal energy state for the new phase: (1) the formation of small regions of lower free energy, and (2) the growth of those regions to a size large enough to propagate to neighboring regions [5]. The presence of "defects" in the material can shorten the time for nucleation of the new phase, but in defect-free material, the time delays for the resulting "homogeneous nucleation" can be significant. This is analogous to the case in which pure water can be superheated in a microwave oven and remain for many seconds until touched or jarred, at which time the water can "explode."

The phenomenon of nucleation of phase changes is critically important for ICF capsules because when homogeneous nucleation is involved, the passage of a shock that superheats the pusher material to as many as several electron volts (eV) will not cause the material to change phase in less than a picosecond, as one might normally expect for several traversals of a lattice spacing by an ion traveling at its thermal speed. Instead, the phase change is delayed for times up to hundreds of picoseconds or even a nanosecond or more, depending on the type of material, the material composition, the shock strength, the degree of superheating, and other factors (especially the resulting pressures) that affect the size of the atomic clusters required statistically to cause regions of lowered free energy to grow large enough to propagate the phase change.

Specifically, for an ICF capsule exposed to an X-ray drive in a hohlraum (or direct drive), the initial portion of the drive temporal profile is generally tailored to launch a shock through the pusher (i.e., through the ablator, if present, and then through the pusher). For pushers whose phase changes are subject to nucleation, the phase-change front follows the shock front at a non-negligible distance as the shock propagates through the pusher, as shown conceptually in Fig. 1, because of the time delay to nucleate the phase change.

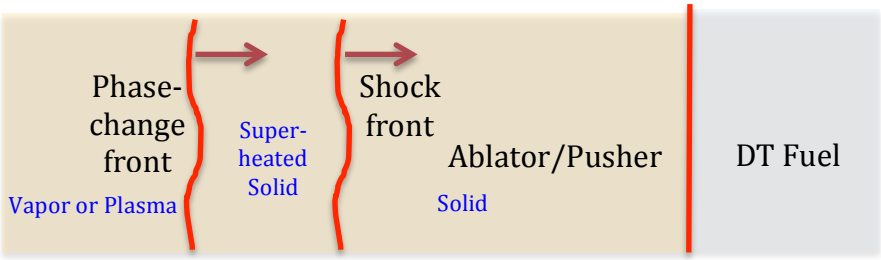

Figure 1. A phase-change front follows a strong shock in a solid metal-like material, leaving a superheated region of solid material between the two fronts.

When the shock reaches the inner surface of the pusher, a rarefaction wave propagates outward back through pusher material that is superheated and compressed *but still in the solid phase*, as shown conceptually in Fig. 2.

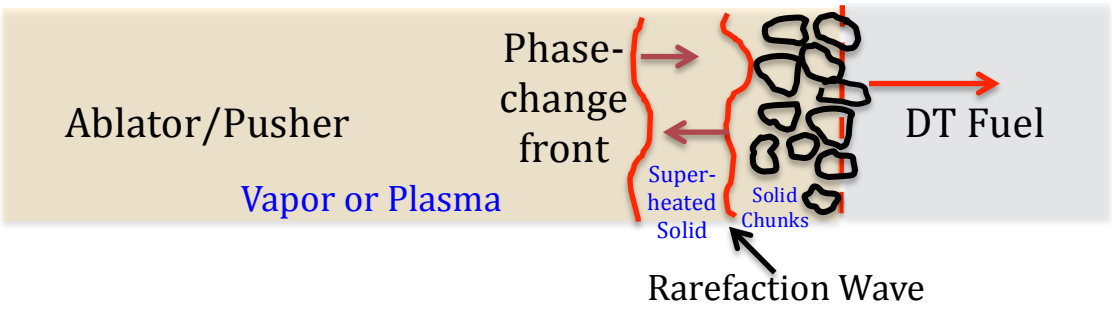

Figure 2. The rarefaction wave created after the shock reaches the pusher-fuel interface travels outward toward the advancing phase-change front. The resultant decompression of the superheated compressed solid pusher material causes spallation of small chunks or "grains" of pusher material into the fuel if the superheated pusher material is subject to differential responses to the rarefaction.

The sudden release of pressure behind the rarefaction wave will cause spallation of chunks of pusher material into the fuel if the material has any sub-structure that acts differentially to the release of the pressure. Factors that typically cause differential responses to sudden decompression of the superheated material are grain boundaries (as for Beryllium), micro-cracking (possibly arising from fuel cryogenic temperatures), stress fractures, etc. Fundamentally, if the material will spall under sudden pressure release, then solid chunks or "grains" of pusher material will be ejected at high speed into the fuel. These chunks can subsequently vaporize while their speeds drop due to "drag" in going through the DT. Such chunks degrade the DT burn much more than RT instabilities because the spalled chunks penetrate into the DT *much farther* (and earlier in time) than RT pusher-DT surface instabilities. Moreover, such spallation occurs essentially independent of any direct dependence on shock strength, at least for the shocks generally required for ICF capsules. Hence, such spallation (when it occurs) is the dominant source of what is typically called "mix" of pusher material into the fuel and/or central DT hot spot. In addition, the departure of small chunks from the pusher leaves the pusher-fuel interface highly perturbed, thus seeding subsequent RT instabilities that might further degrade capsule performance (and possibly affect diagnostic X-ray signals from the hot spot).

Eliminating Spallation Mix

Although spallation-mix physics may be inherent for most modern ICF capsules, we claim that preheating the pusher *inner surface* by a fraction of 1 eV several nanoseconds (or less) prior to arrival of the shock at the pusher-DT interface will liquefy (or vaporize or ionize) that pusher material, thereby *eliminating spallation mix* because no change from the solid phase is coupled to the shock transit. Reiterating, the goal is to employ enough preheat at the inner surface of the pusher to avoid shock transit through *solid* pusher material. Such preheat need not raise the adiabat of the fuel significantly. Thus, the solution to low ICF capsule yields becomes a target-design issue as to how to generate this preheat without significantly raising the fuel adiabat and degrading capsule performance more than necessary. Raising the fuel adiabat is usually thought to be counterproductive to achieving the highest capsule "gain" (i.e., the ratio of the fusion energy produced divided by the energy input) but it may be an unavoidable consequence of the requirement to raise the adiabat of the inner pusher material to avoid significant mix for pushers subject to spallation. Said differently, purposely generating this preheat may allow ignition on the

NIF because it eliminates what is likely to be the dominant mix mechanism. Such preheat could be generated by (e.g.) the use of thin higher-Z layers, material seeding, possibly even a different irradiation wavelength (e.g., at least some 526-nm vs. all 1052-nm drive to generate a small amount of "hot electrons"), or even just a larger initial "picket" on the drive temporal profile (which more recent experiments [1-4] on the NIF are utilizing—we'll come back to this below). The minimum amount of preheat required is whatever is necessary to avoid spallation at the passage of the first strong shock. The only other recourse is to use a pusher that won't spall under shock loading and sudden decompression.

Outline of the Physics of Spallation Mix

To be able to estimate how much burn degradation can be expected for a particular ICF capsule experiment due to spallation mix, we developed the detailed yet very simple physics model described in Appendix A. This model explains how the ejected spallation "chunks" or "grains" propagate into the DT and evolve (via drag, shock heating, etc.) into either an "atomic" or "chunk" mix that can then degrade the fusion burn. Although we indicate below how this model is very accurate in matching data, we emphasize here that a precise knowledge of such a physics model is not necessary, for the following very important reasons:

1. Modern codes now exist that can compute many of the model's effects (e.g., drag) once we know what size of ejecta the spallation produces. The modern codes can also calculate these effects with greater accuracy than is afforded by our phenomenological model. So, if a computational model is desired, the modern computer codes should be used instead of the phenomenological model given in Appendix A.
2. The goal for any experiment is to eliminate spallation mix all together, in which case no modeling of this type of mix is necessary.

Remember, it is only when the inner surface of the pusher is still in its solid state at the passage of the first strong shock that any modeling is required, because otherwise no spallation mix will occur. Future emphasis should thus be on how to design targets that eliminate spallation mix, and not on how to calculate its effects when we fail to eliminate this dominant mix mechanism.

In any case, it is simple to show that any pusher spallation fragments (if in fact ejected into the DT) will penetrate on the order of their own column density of DT (e.g., roughly 0.002 g/cm^2 for 10-micron-size Be grains). Nevertheless, such a "rule of thumb" is too crude, and glosses over the physics that actually describes what occurs. We therefore refer you to the simple phenomenological model described in Appendix A for details, but outline a few features of that model here for the case of a pusher that does tend to spall under shock loading and sudden decompression.

Consider a spherical "single-shell" capsule with a cold pusher subject to a strong shock passage as indicated in Fig. 1. Suppose the pusher is composed of "grains," as for Beryllium. In actuality, these "grains" can be any localized contiguous pusher material isolated by boundaries of any type (grain boundaries, stress fractures, etc.). What we call "grains" can hence be any pusher fragments that can spall as individual roughly round chunks, even though we will consider the example of a Beryllium pusher for clarity of explanation.

For nucleation of the pusher's phase change, note that the shock in Fig. 1 raises the pusher temperature to a few or perhaps tens of eV, and increases its pressure to a few to tens of megabars. At this increased pressure, the clustering effects (e.g., via shared electrons) can

significantly increase the time to form a region of lowered free energy large enough to allow an altered-phase region to spread. This causes the nucleation time for any phase change to be much larger than tens or even hundreds of picoseconds, so a phase-change front will indeed follow the shock front as shown in Fig. 1.

When the shock reaches the pusher-DT interface and initiates a reflected tensile (rarefaction) wave (Fig. 2), the pressure at the interface drops precipitously, and the time to nucleate a phase change would normally shorten drastically. However, the pusher is also cooled greatly because the pusher is decompressed by roughly a factor of four from a high-pressure superheated pseudo-elastic solid to a relatively cold solid. In this cooled state, the grain "boundaries" (which are typically higher-energy states) will melt before the bulk grain material. The tensile wave thus changes the pusher surface next to the DT from a contiguous superheated solid into a bunch of compacted but uncemented solid grains "lubricated" by a matrix of melted grain boundaries. In addition, by dropping the pressure on only the DT side of the tensile wave, the rarefaction causes the grains next to the DT to be accelerated into the DT at high speeds (the expansive forces greatly exceeding the strength of the melted grain boundaries). The speed of the ejected grains ranges from high speed for grains next to the DT to essentially zero speed for grains at the location where the tensile wave meets the phase-change front. Thus, velocity-distributed spallation of relatively cold solid grains occurs whether the DT is a solid, liquid, or a gas. Mix is thus *sure to occur*, and the problem becomes one of calculating how much of the DT is penetrated by the grains based on drag theory and subsequent grain heating (see Appendix A). Moreover, grain ejection creates a very roughened surface that can possibly experience significant RT growth upon deceleration of the pusher near maximum DT compression.

The leading spalled grains are ejected at slightly more than twice the normal free-surface jump-off speed expected from the shock passage. The first "layer" of ejected grains leaves the pusher surface ahead of the shock front that forms thereafter in the DT because the shock front is formed by the rarefaction of the pressurized fluid immediately behind the spalled layer. This rarefaction is not permitted to form until after all grains have been ejected. The leading pusher grains in the rarefaction would normally attempt to leave the pusher at three times the speed of sound in the pusher (just as for adiabatic rarefaction with $\gamma = 5/3$), which is much faster than the ejection speed of the last grains. This means that the shock will reform in the DT in a slightly different manner because some spalled grains will be in the formation region. It also means that the more sluggish grains will be quickly overtaken by this shock. Also note that the reformation time of this DT shock will be delayed (relative to the normal formation time in computer codes ignoring nucleation physics) by the time for spallation of the layer. This time delay is a characteristic signature of the ejection process, and such a delay has been observed experimentally (see below). The leading grains will be out in front of this DT shock, traveling about 3/2 times faster (the shock normally traveling at perhaps 4/3 of the free-surface speed).

The grains entering the DT at such high speed are then subject to hydrodynamic drag. It can be shown that the Mach cones of the leading grains do not "interact" with one another, and hence that it is acceptable to assume that the leading grains enter the DT essentially individually, uninhibited by collective drag effects that might otherwise create a "wall" of grains entering the DT. (If a "wall" were applicable, we might wonder whether the grains could in fact penetrate cryogenic DT---but a "wall" is not applicable). The grains then proceed through the DT much like meteoroids, remaining mostly at near-solid densities, until the main shock catches up to them and causes them to expand to pressure equilibrium with the DT. The grains then form a "chunk mix" in the DT. This chunk mix changes slowly into an atomically mixed state as the DT diffuses into

the grain material by ambipolar ionic diffusion. This diffusion process is very complicated because it occurs during capsule compression, and may not have time to proceed to completion before peak capsule compression occurs. How much capsule yield is degraded by the final state of the mix (chunk vs. atomic) depends on the Z of the pusher and the degree of penetration of the grain material into the DT, as well as the shock history. We found that such degradation is best computed by first computing the radial distribution of pusher material contaminating the fuel regions with one code, and then putting that state into a hydrodynamics burn code. We emphasize that the reason that our simple model is a reasonable approximation for such complicated physics is because the capsule yield generally depends only on the amount of fuel (and/or hot spot) contaminated by the grains before they come to rest via drag and shock transit, and not on the exact radial mass distribution of pusher material in the DT (see Appendix A for the details).

As we indicated above and now re-emphasize, the initial phase of the DT generally *does not matter* because the pusher grains are ejected (spalled) as individual chunks, not as a "wall" of material. Hence, the use of cryogenic DT instead of gaseous DT does not change the spallation-mix process in any significant manner. Besides, cryogenic DT is very likely to be preheated sufficiently to have changed into a fluid at the times of interest. The physics of spallation mix is therefore *inherent* for ICF pushers that are subject to spallation upon the passage of a strong shock.

Phase Explosion in Metals

Studies of laser ablation of metals during the last 15 years involving pulsed nanosecond laser sources have shown that homogeneous nucleation becomes "catastrophic" to an intermediate metastable state of droplets and vapor bubbles when very fast superheating raises the metal's temperature above about 90% of the thermodynamic critical temperature [6,7]. The vapor regions can then grow exponentially in size and subsequently "explode" in what has been termed "phase explosion" that turns the metal into a mixture of droplets and expanding vapor regions [6,7]—but only after a time delay of many nanoseconds [6]. This lag time is contrary to the picosecond phase changes observed at less intense irradiations [8], but is characteristic of the physics of spallation mix. In summary, these laser-ablation experiments may not always involve the exact conditions for ICF, but they experimentally verify the principles of homogeneous nucleation that we incorporate in this paper.

Experimental Proof of Spallation Mix

In Fig. 3, we compare post-experiment predictions of the spallation-mix model described in Appendix A with past ICF hohlraum data from the Halite-Centurion Program [9]. This figure shows that the spallation-mix model agrees with the data better than any other model devised up to the current time. Specifically, the agreement between the model and the data is not only statistically excellent, but no measured yield is higher than what the model predicts by more than 1.4 times the combined |model–measurement| uncertainty. This indicates that spallation mix was the dominant mix mechanism. In particular, we found no RT or RM model able to come anywhere close to predicting these results. For the few experiments that had yields significantly smaller than predicted by spallation mix (i.e., way off the scale to the right in Fig. 3), we assume that other mix mechanisms were dominant according to the list of mechanisms given in the Introduction at the beginning of this paper. No other known mix model can claim this level of success in agreeing

with these experimental data. We therefore believe that such agreement is *strong evidence* for the dominance of spallation mix in most ICF capsules designed and fielded to achieve high yield.

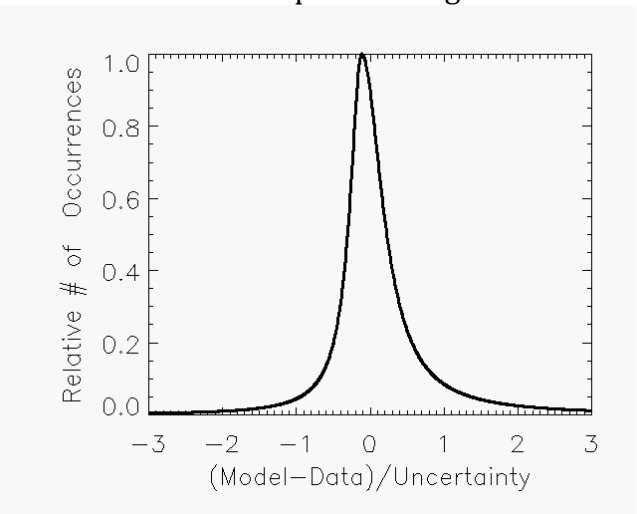

Figure 3. A fit to the histogram of the ratio (Model minus Data)/Uncertainty for the past ICF hohlraum yield data from the Halite-Centurion Program [9] indicates a remarkable match between the model and the measured data. The "Uncertainty" is the RMS of the standard deviations in the model and the data. No nonzero histogram entry was below –1.4 on the abscissa, thus showing that the measured data were never statistically higher than the model. A few nonzero entries were off the scale to the right in the +4 to +7 range, indicating for these capsules that other degradation mechanisms were also at work and not just spallation mix.

One obvious question is whether the success shown by Fig. 3 can be applied to glow-discharge-polymer CH plastic (GDP-CH) ablator-pushers as used for experiments at the NIF. To help answer this question, Dayne Fratanduono of LLNL conducted experiments in July of 2012 on the OMEGA Laser using GDP-CH material and reported peculiar structures both in VISAR (Velocity Interferometric System for Any Reflector) and SOP (Streaked Optical Pyrometer) images, as shown in Fig. 4 [10]. Although investigators have previously considered GDP-CH to be amorphous and homogeneous, such plastic is well known to have internal stresses with a high degree of cross-linking that would tend to make random sub-units making up the "amorphous" structure at the macro scale. Micro-cracking would also be likely for such a material fielded at the NIF against DT of about 20° K. We therefore interpret the evidence shown in Fig. 4 to be the result of spallation from the passage of a strong shock through the GDP-CH plastic.

Similar experiments using pulsed nanosecond 0.7 to 2.2 TW/cm^2 laser irradiation of 150-300-micron-thick films of gold, aluminum, and iron had VISAR effects like those shown in Fig. 4 that the experimenters interpreted to be evidence of spallation [11], just as we have done for Fig. 4. Although the surface effects shown in Fig. 4 utilized GDP-CH placed next to a gas, we again emphasize that the detailed spallation physics presented in Appendix A proves that the occurrence (and dominance) of spallation mix is essentially independent of the initial phase of the DT (cryogenic or gaseous).

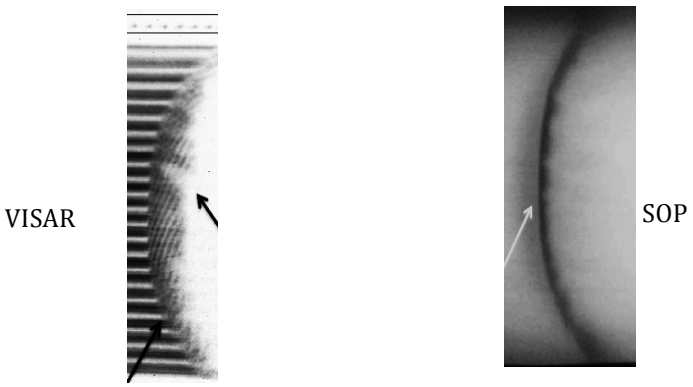

Figure 4. In July 2012, Dayne Fratanduono (LLNL) conducted experiments on the OMEGA Laser by having a strong shock (travelling from left to right) emerge from GDP-CH into methane gas. After the shock formed in the methane and traversed a known distance, it struck a thin silicon nitride film viewed by VISAR and SOP to produce the images shown above [10]. Fratanduono reports that the cause of these strange surface effects is unknown, but we interpret these effects as evidence of spallation from the GDP-CH. These features were not observed for weak shocks.

In addition, experiments on the NIF starting in late September 2013 generated more fusion energy than was supplied to the fuel regions, by increasing the strength of the initial "picket" on the laser drive temporal profile [1-4]. In previous experiments, the "low-foot" laser drive pulse shapes made the capsules have inner pusher temperatures below melting at the first shock transit, but the later "high-foot" experiments [1-4] had inner pusher temperatures near or above the threshold for full melting [12]. The high-foot experiments are hence indirect proof that spallation mix is the dominant mix mechanism for GDP-CH capsule yield degradation, and support our claim that pulse-shape modifications are one way to investigate spallation mix in future NIF experiments.

Also, Regan, et al. [13] fielded a GDP-CH/DT ice capsule at the NIF with mid-ablator Ge-doped layers and a thin inner-most Cu-doped layer. They concluded that ablation-front hydrodynamic instabilities dominated the mix into the central DT hot-spot because they detected highly ionized Ge emissions from the hot spot but no highly ionized Cu emissions, just as calculated for certain ablation-front instabilities [14,15]. However, this experiment may instead be evidence of spallation mix and not ablation-front instabilities because any spalled Cu-doped CH chunks would have been ejected into the DT in a relatively cold state and may not have had time to complete the transition to an atomically mixed *ionized* state (cf. Appendix A Sections J-M). The Ge ionized signal could then have arisen from normal CH-DT interface RT instabilities seeded by the departure of the spalled Cu-doped CH chunks, as described in Appendix A Section L.

Furthermore, the evidence and analysis reported by Barrios, et al. [16] show that "heterogeneous" hot-spot mix (i.e., mix with bright spots on X-ray images of the hot spot) arises predominantly from fill-tube perturbations for some gas-filled Symcap experiments, but arises predominantly from effects other than fill tubes for cryogenic DT and THD targets, as inferred from Fourier PSD analyses of 2010 to 2012 NIF experiments. More recently, Casey, et al. [17] report that gas-filled Symcap experiments at the NIF have revealed "large brightly radiating objects traversing through the hotspot around bang-time, which are likely chunks of CH/CD plastic." Similar observations of X-ray images at OMEGA show titanium dopant from the CH-fuel interface getting into the capsule core by mechanisms that experimenters claim cannot be by either diffusion or radiation-hydrodynamic turbulent mix [18]. We therefore emphasize that

chunks are typical of spallation mix, which can affect hot-spot X-ray emissions, so investigators need to consider this type of mix in their analyses of hot-spot mix.

Conclusions

We have shown how a consideration of homogeneous nucleation of pusher phase change can create a mix of ablator/pusher material into the fuel regions by spallation of small chunks or "grains" ejected from the pusher when the first strong shock transits the pusher-fuel interface. This mechanism is *inherent* whenever (1) the solid pusher adjacent to the fuel changes its phase by nucleation, and (2) such material when shocked (i.e., compressed and superheated, but still a solid) is subject to spallation when suddenly decompressed. Because these two factors are typically true for modern ICF capsules, especially for capsules with metal-like pushers (and apparently also for capsules with GDP-CH plastic pushers), spallation mix is not only expected to occur, but is expected to be the dominant mix mechanism. We believe other mix mechanisms may well contribute, but we emphasize that spallation mix will generally be dominant because the spalled pusher "chunks" *reach much farther into the fuel regions* than the spikes and other perturbations from either RM or RT instabilities acting alone. Besides:

> When capsule surfaces and drive irradiations are made sufficiently smooth, as is possible for modern ICF capsules, hydrodynamic instabilities need not of themselves play a significant role for mix, but spallation mix *will always be a threat* if the pusher material tends to spall under shock loading and sudden decompression.

We have in fact supplied strong evidence for the dominance of spallation mix by a comparison of our spallation-mix model predictions with past ICF data that *cannot* be explained by RT, RM, or other instabilities alone. In particular, no other known mix model can claim the level of success obtained by our spallation-mix model in agreeing with past ICF hohlraum data as shown in Fig. 3.

In addition, we have explained conceptually how spallation mix can be eliminated by either (1) using a pusher that won't spall under shock loading and sudden decompression, or (2) designing ICF targets whose ablator/pusher surface layer next to the fuel is preheated enough to not be in the solid phase when the first strong shock arrives at this location. We therefore emphasize that target design for ICF targets subject to spallation should include a consideration of homogeneous-nucleation physics, and specifically, should eliminate the potential for spallation mix by allowing fuel compressions along slightly raised adiabats in order to *melt the inner surface of the pusher* before the first shock arrives. If this is done, ICF capsule yields will only be subject to the other degradation mechanisms listed in the Introduction of this paper, whose effects need not be significant for suitable target design, modern capsule fabrication technologies, and sufficiently smooth drive irradiations. Thus, elimination of spallation mix is the most important next step in trying to achieve significantly increased ICF capsule yields. Recent experiments at the NIF that have achieved higher yields [1-4] may well be exploring this new design space, so further progress in eliminating spallation mix may well allow "ignition" to be achieved at the NIF.

Acknowledgements

We are thankful for any divine inspiration in developing the spallation-mix model, and are thankful to John Trenholme and Naresh Mehta for reviewing this manuscript. This work (LLNL-

TR-665701) was performed under the auspices of the U.S. Department of Energy by Lawrence Livermore National Laboratory under Contract DE-AC52-07NA27344.

References

1. O. A. Hurricane, et al., "Fuel gain exceeding unity in an inertially confined fusion implosion," *Nature*, Letter, doi:10.1038/nature13008, 00 Month 2014 / Vol. 000.
2. H.-S. Park, et al., "High-Adiabat High-Foot Inertial Confinement Fusion Implosion Experiments on the National Ignition Facility," *PRL*, **112**, 055001 (2014).
3. T. R. Dittrich, et al., "Design of a High-Foot High-Adiabat ICF Capsule for the National Ignition Facility," *PRL*, **112**, 055002 (2014).
4. O. A. Hurricane, et al., "The high-foot implosion campaign on the National Ignition Facility," *Physics of Plasmas*, **21**, 056314 (2014).
5. E.g., F. F. Abraham, Homogeneous Nucleation Theory: The Pretransition Theory of Vapor Condensation, Advances in Theoretical Chemistry, Supplement 1 (N.Y.: Academic Press, 1974); A. S. Michaels, ed., Nucleation Phenomena (Wash. D.C.: American Chemical Society Publications, 1966); and D. Turnbull, Solid State Physics: Advances in Research and Applications, eds. Seitz and Turnbull, Vol. **3** (N.Y.: Academic Press, Inc., 1956) 225-306.
6. Xianfan Xu, "Phase explosion and its time lag in nanosecond laser ablation," *Applied Surface Science*, **197-198** (2002) 61-66.
7. A. Gragossian, S. H. Tavassoli, and B. Shokri, "Laser ablation of aluminum from normal evaporation to phase explosion," *J. Applied Phys.*, **105**, 103304 (2009).
8. E.g., B. Rethfeld, K. Sokolowski-Tinten, and D. von der Linde, "Ultrafast thermal melting of laser-excited solids by homogeneous nucleation," *Phys. Rev. B*, **65**, 092103 (2002) and refs. therein.
9. A joint Los Alamos-LLNL program using nuclear experiments, called Halite at LLNL and Centurion at Los Alamos (collectively called Halite-Centurion), demonstrated excellent performance, putting to rest fundamental questions about the feasibility of achieving high gain. It performed inertial fusion experiments using nuclear explosives at the Nevada Test Site at higher energies than those available in the laboratory.
10. Dayne Fratanduono, LLNL, private communication (April 2014).
11. E.g., E. Lescoute, et al., "Ejection of spalled layers from laser shock-loaded metals," *J. Applied Phys.*, **108**, 093510 (2010).
12. Steve Haan, LLNL, private communication (May 2014).
13. S. P. Regan, et al., "Hot-Spot Mix in Ignition-Scale Inertial Confinement Fusion Targets," *PRL*, **111**, 045001 (July 2013).
14. B. A. Hammel, et al., "High-mode Rayleigh-Taylor Growth in NIF ignition capsules," *High Energy Density Physics*, **6** (2010) 171-178.
15. B. A. Hammel, et al., "Diagnosing and controlling mix in National Ignition Facility implosion experiments," *Physics of Plasmas,* **18**, 056310 (2011).
16. M. A. Barrios, et al., "Experimental investigation of bright spots in broadband, gated x-ray images of ignition-scale implosions on the National Ignition Facility," *Physics of Plasmas*, **20**, 072706 (2013).
17. D. T. Casey, et al., "Development of the CD Symcap platform to study gas-shell mix in implosions at the National Ignition Facility," *Physics of Plasmas*, **21**, 092705 (2014).
18. J. A. Baumgaertel, et al., "Observation of early shell-dopant mix in OMEGA direct-drive implosions and comparisons with radiation-hydrodynamic simulations," *Physics of Plasmas*, **21**, 052706 (2014).

Appendix A: The Orth Simple Model For Spallation Mix

Our simple model of spallation mix is described below as we originated it in 1984-1985. As long as the typical size of the spallation "chunks" is known, this model is based on first principles with no "fitted" parameters. We consider a spherical "single-shell" capsule composed of an outer "ablator," a pusher (that might also serve as the ablator), and an inner "fuel" region of DT in any phase and any layering (i.e., unless stated otherwise, the word "fuel" will refer to any or all of the DT, whether cryogenic with a central DT hot spot or all gaseous). For explanatory purposes, we consider metal-like pushers ranging from Beryllium at low-Z to AuCu at high-Z.

A. Total Column Density Ejected

The total mass ejected by spallation into the DT has a column density of

$$m_{ejected} = 4\rho_p u_t \tau \quad (1)$$

where 4 is the shock compression, ρ_p is the cold density of the pusher material, u_t is the speed of the tensile wave, and τ is the time increment between arrival of the shock at the DT interface and the time the tensile wave meets the phase-change front. Because the phase-change front trails the shock by a distance $u_s\tau_{nucleation}$, where u_s is the speed of the shock and $\tau_{nucleation}$ is the time to nucleate the phase change, we have $u_s\tau+u_t\tau = u_s\tau_{nucleation}$, or

$$\tau = \tau_{nucleation}\frac{u_s}{u_s+u_t} \approx \tfrac{1}{2}\tau_{nucleation} \quad (2)$$

where the last step follows from $u_s \sim u_t$. The ejected mass column density is thus roughly

$$m_{ejected} = 2\rho_p u_t \tau_{nucleation} \quad (3)$$

Note that Be grains ($\rho_p \sim 1.85$ g/cm^3) are typically about 10^{-3} cm in size, and shock speeds are typically about 3-10 cm/μs (i.e., 30-100 μm/ns), so ejection of at least one "row" (i.e., one "layer") of grains requires $\tau_{nucleation}$ to be at least 50-170 ps from the above equation. Also note that the average chord length through a sphere is four times the volume/surface ratio or four-thirds of a radius, so the average column density of spalled material (designated by subscript "sp") ejected into the DT for a spalled layer of average thickness L (which must be at least one-grain size) is

$$\rho_{sp}L_{sp} = \rho_{grain}L_{grain} \approx (4/3)\rho_{grain}r_{grain} \quad (4)$$

B. Speed of Ejected Material Into the DT

The distribution of speeds of the ejected grains is important because it determines where the grains will stop due to hydrodynamic drag. One might suspect that this speed distribution could be easily obtained by analogy to the one-dimensional release of compressed elastic balls originally confined to a box (or a tube). The problem is more complicated than this, however, because the speed of the tensile wave should vary as it crosses the layer to be spalled. That is, the initial speed of the tensile wave, in the frame of the moving material behind the shock, is just the speed of the shock that compressed the material. This speed will decrease, however, as the energetics of the compression are distributed over an increasing thickness of expanding material (in the reverse fashion of trailing disturbances catching up to and reinforcing a shock). We will therefore defer the solution of this important problem for future investigation. Nevertheless, the analogy shows that the leading grains will have the maximum velocity and the last grains to be

ejected will have the minimum velocity (near zero). Energy conservation then requires more grains at slower speeds than faster speeds (because energy is proportional to the square of the velocity), so the distribution of speeds should be peaked toward the slower speeds.

Lacking the correct solution for the distribution of speeds (which will turn out to be unimportant), we will make the following crude arguments to obtain the maximum spall speed v_0, which is the speed of the first "row" of grains. First note that the average compressional energy per unit mass due to the shock defines a characteristic speed u_0, as specified in the frame moving at the material speed u_m established by the shock with pressure P_{pusher} [A1]:

$$(1/2)\,u_0^2 = (3/8)\left[\frac{P_{pusher}}{\rho_{pusher}}\right] \tag{5}$$

This u_0 is equal to u_m, and would be the speed of the leading grains were it not for the decompression of the second row of grains. Their decompression supplies additional force to accelerate the leading grains. The decompressions of additional rows also contribute through forces on the intermediate rows. The leading grains are thus accelerated until their speed "outruns" the decompression, in the sense that their speed is equal to the product of the speed of the tensile wave and the decompression ratio. If we assume that the speed of the tensile wave decreases only to u_0 given by Eq. (5), and assume that the strong-shock decompression ratio is a factor of 4, then the speed of the leading grains would be $4u_0$ in the material frame, or $5u_0$ in the capsule frame:

$$v_0 \cong 5u_0 = (5/2)\sqrt{3\,P_{pusher}/\rho_{pusher}} \tag{6}$$

For convenience in extracting information for our theory from computer-code calculations, we want to express Eq. (6) in terms of the normal speed of the interface between the pusher and the DT (i.e., the free-surface jump-off speed in the case of the gaseous materials *incorrectly* assumed in presently used hydrodynamics codes). This interface speed is [A2]

$$u_{Free\ Surface} = \sqrt{\frac{2P_{DT}}{(\gamma+1)\rho_{DT}}} \tag{7}$$

where P_{DT} is the pressure of the shock established in the DT, and ρ_{DT} is the original DT density. Assuming $\gamma = 5/3$, and defining $\xi = P_{DT}/P_{pusher}$, we obtain the ratio as

$$\left(v_0/u_{Free\ Surface}\right) = 5\sqrt{\frac{\rho_{DT}}{\xi\rho_{pusher}}} \tag{8}$$

The transcendental equation for ξ is [A3]

$$1 + \sqrt{5}\left(1-\xi^{1/5}\right) = \sqrt{\frac{\xi\rho_{pusher}}{\rho_{DT}}} \tag{9}$$

An approximate solution of this equation for parameter values of interest is

$$\xi = 2.5\left(\rho_{DT}/\rho_{pusher}\right)^{0.88} \quad (10)$$

The ratio in Eq. (8) thus becomes

$$\left(v_0/u_{Free\ Surface}\right) \cong 3.2\left(\rho_{DT}/\rho_{pusher}\right)^{0.06} \quad (11)$$

For typical values of the pusher and DT densities for metals (e.g., Be, AuCu), this ratio is about 9/4. This might be somewhat too high because we have ignored any inelasticity in the compressed pusher (which may in fact be okay), and we have ignored any possibility of the tensile wave slowing down to a speed less than u_0 in the distance of interest. The latter may also be okay, but the eventual speed of the tensile wave, given sufficient distance of propagation, would of course be just the speed of sound. We also note that the total variation in this ratio for typical ICF capsules is probably 2.1 to about 2.4. Considering all of the uncertainties, we simply assume that the ratio is exactly 2:

$$\left(v_0/u_{Free\ Surface}\right) \equiv 2 \quad (12)$$

Thus, we assume that the leading spalled grains are always ejected at exactly twice the normal free-surface jump-off speed. We emphasize that future investigation should calculate this ratio with greater accuracy.

C. Spalled Grains Enter the DT Ahead of the Shock

The first row of ejected grains leaves the pusher surface ahead of the shock front that finally forms in the DT. The reason for this is that the shock front is formed by the rarefaction of the gaseous pressurized fluid immediately behind the spalled layer. This rarefaction is not permitted to begin until after all grains have been ejected. The leading pusher molecules in the rarefaction would normally attempt to leave the pusher at three times the speed of sound in the pusher (just as for adiabatic rarefaction with $\gamma = 5/3$), which is much faster than the ejection speed of the last grains. This means that the shock in the DT will form in a slightly different manner because some spalled grains will be in the formation region. It also means that the more sluggish grains will be overtaken by this shock very quickly. Also note that the formation time of the DT shock will be delayed (relative to the normal formation time in computer codes operating without nucleation physics) by the time for spallation of the layer. This time delay is perhaps one characteristic signature of the ejection process. In any case, the leading grains will be out in front of this DT shock, traveling about 3/2 times faster (the shock normally traveling at 4/3 of the free-surface speed).

D. Overview of Hydrodynamic Drag Deceleration

We must now calculate how the ejected grains decelerate through momentum interactions with the DT. We will focus only on the leading grains, for several reasons. First, the proper treatment for the other grains is much too difficult to be considered here, especially since there are undoubtedly collective drag effects and we have not yet calculated the ejection speeds of these other grains. Second, the leading grains are the ones that penetrate the most DT before stopping because they are ejected with the highest velocities. They are hence the grains that set the maximum depth of original fuel that becomes contaminated with mix originating from the

spallation mechanism. Third, we will find that most yield degradation is established by treating an outer contaminated-fuel region surrounding an inner "clean" fuel region (if present) with the contaminated region defined by how far the leading grains penetrate the DT (fuel and/or hot spot). We will therefore calculate the trajectories of these leading grains, in terms of their position in capsule radius as a function of time.

The drag problem at hand is hence that of an array of solid grains that were originally the first "row" (or first couple of "rows") of grains along the pusher-DT interface, and are now moving supersonically out into the relatively cold DT at speed v_0. Each grain will have its own oblique shock, much like the V-shaped shock from a supersonic airplane moving through air. For an array of grains all moving at v_0, we might wonder whether the row acts like a near-solid wall. This is not the case, however, because we will show that the Mach cones of the grains do not interact. We shall therefore assume that the DT is able to flow easily around each of the leading grains, due to differential velocities or whatever, and that each grain can be treated as *an isolated problem* in drag theory.

To show that the Mach cones do not interact, note that the Mach number M of the grains entering the DT is the ratio of v_0 and the speed of sound in the cold DT,

$$M \approx 3\sqrt{\frac{(P_{pusher}/\rho_{pusher})}{(P_0/\rho_{DT})}} \qquad (13)$$

Here P_0 is the pressure in the ambient (preheated) DT, (P_0/ρ_{DT}) may be about 10^4 Joules/g, and $(P_{pusher}/\rho_{pusher})$ may be about 10^6 to 10^7 Joules/g. Typical values for M may thus be about 30 to 100. The half-angle of the Mach cone, being the inverse sine of 1/M, is thus only about 2 degrees or less. This fact supports the view that the Mach cones of the leading grains do not "interact" with one another, and hence that it is acceptable to assume that the leading grains enter the DT essentially individually, uninhibited by collective drag effects.

E. Grain Vaporization Inside the DT

The next question we must consider is for how long the grains remain solid along their trajectories. We might at first expect the grains to be vaporized very quickly because the temperature in front of a grain and behind the Mach cone is roughly the product of one-fifth of the ambient DT temperature (perhaps as much as ½ to 1 eV) and the square of the Mach number [A4]. Because we have already shown that the Mach number is initially about 30 or more, we expect initial peak temperatures near or above 100 eV. Most any grain immersed in such a temperature bath would quickly ionize and disperse. The hot DT inside the Mach cone is not optically thick, however, so this DT does not act as an efficient temperature bath. There are also a number of cooling mechanisms whose effects are very important. For example, the maximum grain energy input rate from DT collisions is $[(1/2)m_{DT}v^2](\pi r_{grain}^2)n_{DT}vC_D = 1.6\ r_{grain}^2v^3C_D\rho_{DT}$ jerks/shake, where v is in cm/shake, n_{DT} is the number of D or T per unit volume, C_D is the drag coefficient (to be specified below), one shake is 10^{-8} second (10 ns), and a jerk is 10^9 Joules. The whole spherical surface radiation rate is $(4\pi\ r_{grain}^2)\sigma T^4 = 13\ r_{grain}^2T_{keV}^4$ jerks/shake. If we equate these two rates and estimate v as v_0 times ½ to 1, v_0 as perhaps 1/3 cm/shake, C_D as ½, and ρ_{DT} as 0.002 to 0.02, we find that the peak grain temperature is limited by surface radiation in typical ICF capsules to somewhere between 25 and 85 eV *independent of radius*. Another cooling mechanism occurs because the DT moving behind the Mach cone carries away the equivalent heat resulting from the acceleration of ablated "vaporized" grain particles up to the DT wake speed as they are swept off

the grain. Also, some heat goes into volume heating of the grain. Whether the grains vaporize or not is therefore a very complicated question best left to computer calculations.

Nevertheless, we here assume that the same thing happens to grains as happens to meteoroids, namely, they slowly ablate away at their surface. That is, as a grain decelerates, its front surface begins to ablate. The material leaving the grain is accelerated to near-DT wake velocities as it is pushed behind the grain by the DT. This material loss acts to cool the grain, as does radiation. We further assume that the grain "rotates" enough to avoid becoming flattened, and the whole surface of the grain thereby participates occasionally in the ablation process. Meanwhile, the center of the grain remains solid. The important question is how fast the ablation occurs in comparison to the overall hydrodynamic deceleration rate. The solution to this interesting question is beyond the scope of this work, but future investigation should definitely answer this question. The ablation will certainly reduce the column density of the grains by some amount, but probably by less than the uncertainty that already exists here due to the lack of knowledge of the grain size distribution. Also, significant mass-loss rate occurs only during the time the grains are moving fast. We therefore assume that the grains remain solid and that their column densities are not altered in the capsule's radial direction (which is certainly not correct, but sufficiently accurate here).

F. Drag Theory of Grain Stoppage In the DT

For simplicity, we here assume that the path of each of the leading grains is entirely in the capsule's radial direction. We also assume that the effective density and temperature conditions behind each Mach cone are the same as behind the main shock in the DT (for the purpose of calculating viscosities and thus Reynolds numbers). The conditions of course may vary from hotter temperatures and higher densities immediately in front of the grains (which are moving 3/2 times faster than the shock) to much lower conditions at the sides and back behind the grains. The approach taken here is thus very crude, but our results are rather insensitive to Reynolds number, so it doesn't matter much.

With the above simplifying assumptions, we can now start with the normal hydrodynamic drag equation

$$m_{sp}(dv/dt) = -C_D a_{sp}[(1/2)\rho_{DT} v^2] \qquad (14)$$

where "sp" refers to spallation, m_{sp} is the mass of a spalled grain, v is the instantaneous speed of the grain, t is the time elapsed after grain ejection, C_D is the drag coefficient specified by the DT conditions behind the Mach cone, a_{sp} is the cross-sectional area of the grain transverse to the direction of motion, and ρ_{DT} is the initial DT density (because the bracket expression applies to the DT in front of the Mach cone, as seen in the rest frame of the grain). The ratio of the mass and cross-sectional area will be specified in terms of the column density of the spalled material in the capsule's radial direction via Eq. (4):

$$m_{sp}/a_{sp} = \rho_{sp} L_{sp} \qquad (15)$$

The drag coefficient on spherical bodies, for low Mach numbers, is given approximately by [A4]

$$C_D \cong \left[(24/R) + 0.5\left(1 + e^{-0.002R}\right)\right] \qquad (16)$$

where R is the Reynolds number. For the accuracy desired here, it is expedient to ignore the minor changes in C_D for high Mach numbers [A4] and also to neglect the exponential term:

$$C_D \approx [0.5 + (24/R)] \tag{17}$$

The second term in Eq. (17) is what converts Eq. (14) to Stokes flow. Putting Eq. (17) into Eq. (14), separating the velocity terms, and integrating, we obtain

$$v = \frac{v_0}{\left[\{(R_0/48)+1\}exp\left(\frac{12\rho_{DT}v_0 t}{\rho_{sp}L_{sp}R_0}\right)-(R_0/48)\right]} \tag{18}$$

where R_0 is the initial Reynolds number

$$R_0 = \frac{2v_0 r_{grain}}{\kappa} \tag{19}$$

Here κ is the kinematic viscosity in cm^2/shake [A5],

$$\kappa = \frac{1.6x10^{-5}T_{keV}{}^{+5/2}}{(\rho^*_{DT})(ln\Lambda_{DT})} \tag{20}$$

where $\rho_{DT}^* \approx 4\rho_{DT}$ behind the Mach cone. The DT Coulomb logarithm is

$$(ln\Lambda_{DT}) = ln\left[\frac{4.9x10^{14}T_{keV}^{3/2}}{Z_{DT}^2 n_e^{1/2}}\right] \cong ln\left[\frac{500T_{keV}^{3/2}}{\sqrt{\rho_{DT}}}\right] \tag{21}$$

and may be typically between 3 and 7, with n_e being the electron density. The last step in Eq. (21) uses the original DT density by assuming the DT near the spalled material is compressed by a factor of about 4. The initial Reynolds number is thus

$$R_0 = \frac{5x10^5 r_{grain}v_0(ln\Lambda_{DT})\rho_{DT}}{T_{keV}^{5/2}} \tag{22}$$

where the units of r_{grain}, v_0, and ρ_{DT} are cm, cm/shake, and g/cm^3, and T_{keV} is the DT temperature in keV behind the main shock just as it passes the pusher-DT interface.

G. Amount of DT Penetrated By Spalled Material

Inserting the above equations into Eq. (18) and integrating, we obtain the leading grain trajectory as the following:

$$r = r_0 - \left(\frac{4\rho_{sp}L_{sp}}{\rho_{DT}}\right)\left\{ln\left[\{(R_0/48)+1\}e^{+wt} - (R_0/48)\right] - wt\right\} \tag{23}$$

where

$$w = \frac{12\rho_{DT}v_0}{\rho_{sp}L_{sp}R_0} \tag{24}$$

Defining $\Delta r = (r\text{-}r_0)$ as the radial distance penetrated by the leading grains in the initial capsule configuration (i.e., before compression), we obtain the column density of DT penetrated by the spallation material as

$$\rho_{DT}\Delta r = 4\rho_{sp}L_{sp}\left\{ln\left[\{(R_0/48)+1\}e^{+wt} - (R_0/48)\right] - wt\right\} \tag{25}$$

To use this equation, we must set $t = t_{STOP}$ as determined for each capsule (usually) by finding where the main shock trajectory intersects the leading grain trajectory given by Eq. (23), as described in the next Section. For capsules in which spallation is the dominant mix mechanism, Eq. (25) determines the extent of the fuel mixed with pusher material because the relative column densities of mixed and clean fuel *do not change* with further capsule compression.

H. Calculation of t_{STOP} via Hydrodynamic Expansion of the Grains

The leading grains follow a trajectory given by Eq. (23) and contaminate a column density of DT given by Eq. (25), but only up to time $t = t_{STOP}$ when the grains stop. We now show that the stoppage time t_{STOP} is determined by the time at which the grains suddenly heat up throughout their entire volume, and expand to pressure equilibrium with the DT.

Volumetric heating of the grains can occur on a time scale of interest only through the heating of the entire region of DT surrounding the grains. The DT is the only sufficient source of heat because we have already assumed that the heating of a grain from its own oblique shock is confined to the grain's surface, and direct radiative coupling of energy from out in front of the main shock to a grain should be relatively minor in terms of the heating required. In addition, the scale length of the electron temperature gradient in front of the main shock is usually sufficiently small that direct grain heating does not occur until the main shock is actually in the process of "passing" the decelerating grain.

The grains are thus heated by the DT, and this heating typically occurs when the main shock passes the grain. The heated DT then causes the grain to ablate, heat, and expand to temperature and pressure equilibrium with the DT in less than nanoseconds. These processes create a "chunk" mix of pusher material surrounded by compressed DT. The exact state of this chunk mix is slightly different depending on whether the grains heat up and expand before the arrival of the main shock, or whether they heat up and expand more typically after being shocked. Because the exact configuration of chunk mix is relevant only for the lower-Z pushers, and because such materials (e.g., Be) generally do not expand until after shock passage, we will hereafter assume that the hydrodynamic expansion occurs after the passage of the main shock. The grain expansion thus occurs in DT that has been shocked to about 4 times its original density.

With this assumption, the densities of the grains and DT after grain expansion can be computed from simple mass = volume x density relations, and the fact that pressure and temperature equilibrium requires the ratio of densities to be equal to the inverse ratio of (Z+1)/A factors because $P = 0.1\rho T(Z+1)/A$ for atomic number Z and atomic weight A. If we assume that "y" times as much pusher mass infiltrates a given mass M_{DT} of DT, then

$$M_{DT} = \rho_{DT}^{**}V_{DT}^{**} = 4\rho_{DT}\left(V_{DT}^{**} + V_{sp}^{**}\right) = 4\rho_{DT}V_{DT}^{**}\left[1 + \frac{\rho_{DT}^{**}y}{\rho_{sp}^{**}}\right] \tag{26}$$

where the post-expansion densities are

$$\rho_{DT}^{**} = 4\rho_{DT}\left[1 + \frac{y(Z_{sp}+1)}{0.8A_{sp}}\right] \quad (27)$$

$$\rho_{sp}^{**} = 4\rho_{DT}\left[y + \frac{0.8A_{sp}}{(Z_{sp}+1)}\right] \quad (28)$$

where the asterisks signify a time frame after grain expansion, and Z_{sp} is the effective spalled charge state. For Be and y = 1, typical values may be $\rho_{DT}^{**} \cong 7\rho_{DT}$ and $\rho_{sp}^{**} \cong 10\ \rho_{DT}$. The hydrodynamic expansion decreases the spalled density by a factor of $(4\rho_{pusher}/\rho_{sp}^{**})$, which may be a factor of 40 to 400 for Be grains, and 20 to 200 for AuCu grains.

The grain density decrease from the hydrodynamic expansion increases the effective drag on the grains by a huge amount. To see this, first note that spherical grains end up pancaked in the capsule's radial direction after shock passage. The shock compression does not change $\rho_{sp}L_{sp}$ because the density and length are altered by equal but reciprocal factors. The pancaked grains then begin their expansion in the hot DT behind the shock. The first factor of about 4 increase in volume also preserves $\rho_{sp}L_{sp}$ because a pancake expands most in the direction transverse to its plane. The remaining density decrease by a factor of perhaps 10 to 100 does decrease $\rho_{sp}L_{sp}$ because this part of the expansion is essentially spherical. The column density of the spalled material therefore decreases by the two-thirds power of just this part of the density change. The column density of the spalled material is thus reduced by a factor of perhaps 5 to 20, and the "range" of the grains is reduced by approximately the same factors (cf. Eq. 25). In addition, when the main shock passes the grains, the drag force increases by the increase in DT density in front of the grains (cf. Eq. 14), which is a factor of about 4 for strong shocks. It is for both of these reasons that the grains come to an abrupt halt when the grains are overtaken by the main shock. This is hence the time of t_{STOP}.

The importance of the increase in drag occurring after the main shock front passes the grains is rather obvious if we take the limit of Eq. (25) for large t under the opposite assumption that the shock never passes the grains. In such a case (which is of course not likely) and t were allowed to become very large, the limit of Eq. (25) would be

$$\rho_{DT}\Delta r < 4\rho_{sp}L_{sp}ln[(R_0/48) + 1] \quad (29)$$

For typical values of R_0 of 100 to 1000, $\rho_{DT}\Delta r$ would then be 4 to 12 times $\rho_{sp}L_{sp}$, not the usual 1 to 2 time $\rho_{sp}L_{sp}$. Thus, the effect of the shock passage is very important.

I. Effective Radius of an Expanded Grain

For the grain-DT two-component expansion described above, the grain radius scales as the cube root of that part of the density increase in excess of 4. We thus obtain the expanded grain radius from Eq. (28) as

$$r_{expanded} = r_{grain}\left[\frac{(\rho_{pusher}/4\rho_{DT})}{\left\{y + \frac{0.8A_{sp}}{(Z_{sp}+1)}\right\}}\right]^{1/3} \quad (30)$$

The ratio ($r_{expanded}/r_{grain}$) then varies typically from perhaps 4 to 10 for Be and 7 to 15 for AuCu for all small values of y.

The total equivalent spherical volume of both the grains and the DT which is in effect assigned on the average to each expanded grain has a radius given by

$$h = \left[\frac{V_{mixed}^{**}}{(4/3)\pi N_{grains}}\right]^{1/3} \tag{31}$$

where V_{mixed}** is the total volume of shocked grain and DT material in the mixed region, and N_{grains} is the total number of pusher grains injected. Assuming that "y" times as much pusher mass is injected as there is DT mass in V_{mixed}**, we obtain

$$N_{grains} = \frac{yM_{DT}}{m_{grain}} = \frac{4y\rho_{DT}V_{mixed}^{**}}{(4/3)\pi r_{grain}^3 \rho_{grain}} \tag{32}$$

where $\rho_{grain} \cong \rho_{pusher}$. Inserting Eq. (32) into Eq. (31), we obtain

$$h = r_{grain}\left[\frac{\rho_{pusher}}{4y\rho_{DT}}\right]^{1/3} \tag{33}$$

The mass ratio "y" is very important in determining the degradation of the burn in the mixed region. The minimum value of y occurs at the interface between the mixed region and the clean DT, because the mixed mass distribution peaks toward the pusher as a result of the ejected velocity distribution being peaked toward smaller velocities. We can estimate this minimum value of y very crudely by first assuming that the spalled material is stopped after traversing its own column density of DT. The average enhancement due strictly to the spherical geometry is then $4\pi r_0^2\rho_{DT}\Delta r$ divided by $(4\pi/3)\rho_{DT}[r_0^3-(r_0-\Delta r)^3)]$, where r_0 is the initial DT radius, or,

$$y = \frac{1}{\left[1-(\Delta r/r_0)+(1/3)(\Delta r/r_0)^2\right]} \tag{34}$$

Minimum y values are typically between 1 and 2 when allowances are made for the column densities traversed by the spalled grains, as well as where in radius such traversals occur.

J. Diffusion Processes to Produce Atomic Mix

In the previous Section, we described how the spalled grains expand very quickly to pressure equilibrium with the DT and stop when they are heated sufficiently, with that heating usually occurring when the main shock catches up to and passes the decelerating grains. Immediately after hydrodynamic expansion from the shock passage, the mixed region is composed of a chunk mix of pusher material surrounded by compressed DT. For high-Z pushers, this is the last stage we need consider because the burn doesn't care what type of mixed state the high-Z material is in. In contrast, the burn mode depends drastically on the type of mixed state for low-Z pushers like Beryllium, as we will explain in Section L. We therefore consider here what happens to a chunk mix involving low-Z material as time progresses beyond this point.

As we might expect, a chunk mix changes slowly to an atomically mixed state as the DT diffuses into the spalled-material regions by ambipolar ionic diffusion. This diffusion process is

very complicated because it occurs during capsule compression. The dynamics of the compression distort the sphericity of the expanded grains due to the passage of shocks, and greatly alter the diffusion rate as the temperature around the grains is increased first due to compression and then due to the onset of burn. We shall approximate the true diffusion situation, which changes as a function of time, by first considering an idealized problem with fixed boundary conditions and fixed densities and temperatures. We shall then alter the solution of this simplified problem to approximate the true situation. We will also totally neglect the time required for the shocked grains to expand to pressure equilibrium with the DT and begin the diffusion stage. Caution must thereby be exercised if applying this spallation theory to capsules with very weak main shocks and grains that require a lot of heating before they will ablate and heat up.

We describe the simplified diffusion process by the following equation:

$$\nabla P_s + \left[\frac{Z_s n_s}{\sum_i Z_i n_i} - \frac{m_s n_s}{\sum_i m_i n_i}\right] \nabla P_e - \left[\frac{m_s n_s}{\sum_i m_i n_i}\right] \nabla\{\textstyle\sum_i P_i\} \cong Q m_s n_s \left(\vec{v} - \overrightarrow{v_s}\right) \tag{35}$$

where P is pressure, Z is effective charge (i.e., Z-"bar"), m is mass, n is number density, v is the mean fluid velocity, and subscripts s, i, and e refer respectively to the ions whose diffusion is under study, any ion species, and electrons. We may express Q as the following:

$$Q = (4/3)\sqrt{2\pi}(ln\Lambda)e^4(kT)^{-3/2}\left[\textstyle\sum_i n_i Z_i^4 (2m_i)^{-1/2}\right] \tag{36}$$

where lnΛ is the mean Coulomb logarithm for all ion-ion interactions, k is Boltzmann's constant, e is the electronic charge, and T is the fluid temperature. For our applications, the total-ion-pressure term and the electronic pressure-gradient term in Eq. (35) are both very small. The number density flux is thus

$$n_s\left(\overrightarrow{v_s} - \vec{v}\right) \cong -\nabla P_s / m_s Q = -(kT/m_s Q)\nabla n_s = -D\nabla n_s \tag{37}$$

so the diffusion constant D is

$$D = kT/m_s Q \tag{38}$$

Now consider a spherically symmetric problem consisting of a sphere of expanded grain material surrounded by an envelope of DT. The time required for the DT to diffuse into the center of the grain material is approximately equal to the time needed for the grain material to diffuse out into the DT, due to the ambipolar nature of the diffusion. That is, the electronic pressure gradient prevents the more mobile D and T from diffusing much faster than the heavier ions. Although the tritons are slightly faster, and the deuterons are even faster, the time constants are all nearly the same. We will therefore calculate the time constant by considering the spalled material diffusing out into the DT. Note that the problem we must solve is hence the diffusion of grain material through the DT and out to a fixed boundary set by the average volume of DT delegated to each expanded grain globule. We shall approximate this constraining boundary as a sphere for simplicity. The applicable spherically symmetric diffusion equation is

$$\frac{\partial n_s}{\partial t} = D\nabla^2 n_s = (D/r^2)\frac{\partial}{\partial r}\left[r^2\frac{\partial n_s}{\partial r}\right] \quad (39)$$

Choosing $n_s = n_0 + T(t)N(r)$ to separate the variables, we find the time-dependent solutions to be

$$T(t) = Ae^{-t/\tau} \quad (40)$$

The radial equation becomes

$$r^2N'' + 2rN' + (r^2/\tau D)N = 0 \quad (41)$$

whose solution is the zeroth-order spherical Bessel function [sin(z)/z] with argument $z = [r/(\tau D)^{1/2}]$. The constraint that the total number of grain ions must be constant, independent of time, requires

$$\int_0^{[h/\sqrt{\tau D}]} dz\, 4\pi z^2\ \sin(z)/z = 0 \quad (42)$$

whose non-zero solutions satisfy

$$tan\left[h/\sqrt{\tau D}\right] = \left[h/\sqrt{\tau D}\right] \quad (43)$$

where "h" is the radius of the total volume of DT and grain material assigned to one grain after hydrodynamic expansion (cf. Eq. 33). The complete solution is thus

$$n_s = n_0 + \sum_j C_j\, exp\left[-t/\tau_j\right]\ \frac{sin[r/\sqrt{\tau_j D}]}{[r/\sqrt{\tau_j D}]} \quad (44)$$

where each term corresponds to the successive non-zero solutions of Eq. (43), that is,

$$\left[h/\sqrt{\tau_j D}\right] = 4.493, 7.725, 10.904, \ldots \quad (45)$$

The slowest-dying mode has the largest τ_j, which corresponds to the first solution in Eq. (45), so the time constant for the diffusion of the grain out into the DT is

$$\tau_{Diffusion} = \tau_1 \cong \frac{h^2}{(4.493)^2 D} \quad (46)$$

We now want to insert Eq. (36) into Eq. (38), and Eq. (38) into Eq. (46). First we note that the n_i in Eq. (36) refer to the ion densities at the grain-DT "interface" where the diffusion is actually occurring. Realizing that there is some ambiguity in the location of this "interface" along the gradients in n_i, we choose $n_i = \rho_i^{**}N_{Av}/A_i$ with $\rho_i^{**} = w_i\,\rho_{Mean}^{**}$ for fractional weights w_i. Then, using $m_i = 1.66\text{x}10^{-24}A_i$ and adjusting the units, we obtain

$$\tau_{Diffusion} \cong 4700\, h^2 A_{sp}(ln\Lambda)\rho_{Mean}^{**}T_{STOP}^{-5/2}\left[\sum_i \frac{Z_i^4 w_i}{A_i^{3/2}}\right]\ \ shakes \quad (47)$$

where the sum runs over D, T, and the grains. Note that h in Eq. (47) is given in centimeters by Eq. (33), T_{STOP} is the temperature environment of the spalled material in keV after time t_{STOP}, and the Coulomb logarithm

$$ln\Lambda = ln\left[\frac{4.9x10^{14}\,T_{STOP}^{3/2}}{Z_{sp}Z_{DT}\sqrt{n_e}}\right] \tag{48}$$

is about 4 ± 1 for Be for typical ICF conditions. Here ρ_{Mean}** is approximately the mean (grain+DT) density at their "interface" at some representative time. For an equal-mass mixture of pusher and fuel, the mean density after hydrodynamic expansion is about 8 times the original DT density. In the general case in which the ratio of pusher and DT masses in the contaminated region is labeled "y", we can use ρ_{Mean}** in Eq. (47) as the approximate average of the two densities in Eq. (27) and (28) in g/cm^3:

$$\rho_{Mean}^{**} \cong 2\rho_{DT}\left(Z_{sp} + 0.8A_{sp} + 1\right)\left[\frac{1}{(Z_{sp}+1)} + \frac{y}{(0.8\,A_{sp})}\right] \tag{49}$$

where as usual, "sp" refers to the spalled grain material.

Equation (47) is only a slowly increasing function of y. For example, for Be, it would contain the factor $(0.85y+1.22)/y^{2/3}$ from Eqs. (33) and (49), which is 2.07 for y = 1, but drops to 1.81 for y = 3, and increases to only 2.47 by y = 20; the summation factor in Eq. (47) increases approximately as y/(y+1), which can increase by at most a factor of two. The diffusion time is hence not very sensitive to the total amount of pusher mass injected as spalled material.

K. Some Complexities of Reality

We must now alter Eq. (47) to include some of the complexities of reality. First note that subsequent capsule compression (which is spherical) will increase the mean density by some factor and decrease h by the 1/3 power of this same factor. Hence, capsule compression beyond t_{STOP} will increase the diffusion time by the cube root of the density increase in the DT at the location of the grains. Second, note that subsequent shocks will increase the mean density and decrease h by about the same factors, so shocks passing the spalled region after t_{STOP} will decrease the diffusion time by the same factor by which the DT density is increased (i.e., up to a factor of 4). Third, note that Eq. (47) is very sensitive to the grain temperature, primarily through the $T^{-5/2}$ factor (we will ignore the slight effect from Z_{sp} in the sum). Temperature increases due to capsule compression and shocks will therefore shorten the diffusion time by very significant factors. Fourth, note that the onset of burn will compress the remaining spallation pockets and essentially terminate the diffusion stage by decreasing h.

We can obtain a measure of the actual diffusion time by integrating the reciprocal of Eq. (47) using the following expression:

$$x_{Diffusion} = \int_{t_{STOP}}^{t_{BURN}} \frac{dt}{f(t)\,\tau_{Diffusion}} \tag{50}$$

where f(t) contains all appropriate density and temperature factors, and t_{BURN} is the time when "significant" burn first begins. Empirically, t_{BURN} can be estimated as the later of (1) the time when the burn rate exceeds 10^{-5} jerk/gram/shake (where 1 jerk = 10^9 Joules), or (2) the time just after complete passage of any strong shock. To continue, we rewrite Eq. (50) as follows:

$$x_{Diffusion} = \left(\frac{1}{\tau_{Diffusion}}\right) \int_{t_{STOP}}^{t_{BURN}} dt \left(\frac{\rho_{STOP}}{\rho}\right)^{1/3} \left(\frac{T}{T_{STOP}}\right)^{5/2} \prod_{i=2}^{n} \left[1 + \left(x_i^{4/3} - 1\right) U\left(t - t_i\right)\right] \quad (51)$$

where n is the number of strong shocks passing the grains (i = 1 referring to t_{STOP}), U(t-t_i) is the unit step function, and x_i is the density change at the passage of the i^{th} shock. The product factor merely introduces multiplicative factors of $x_i^{4/3}$ for each shock passing the grains after t_{STOP}. Note that $x_{Diffusion}$ is a measure of the completeness of the diffusion stage; that is, $x_{Diffusion} < 1$ indicates that chunk mix is still present, $x_{Diffusion} \sim 1$ indicates that the mix is mostly atomic, and $x_{Diffusion} >> 1$ indicates complete atomic mix.

L. RM and RT Instabilities

RM and RT instabilities are more than just possible contributors in the hierarchy of mix mechanisms. They are almost certain to occur for suitable deceleration profiles near peak compression because the ejection of grains will leave the inner surface of the pusher very roughened.

When a second or third shock transits the pusher-DT interface, RM instabilities may occur. There may even be shaped-charge-like ejection of material from already-formed perturbations with steep sides, but such ejection is a form of the RM instability. Later in the capsule's compression when the DT decelerates the pusher, RT instabilities may definitely occur. The effect of the RM and RT instabilities will vary from capsule to capsule because these processes depend on the detailed acceleration and deceleration history of the pusher-DT interface. In most cases, however, the result is to introduce pusher material (e.g., spikes) having a geometrical structure that is very elongated in the radial direction. These objects will therefore expand primarily in their transverse direction to reach pressure equilibrium with the DT, and will thus have *very small radial column densities*. It is rather obvious that such objects will usually not traverse much fuel in terms of g/cm^2. Thus, for pushers composed of moderate-sized grains, spallation mix will tend to dominate the total depth of fuel contaminated, but RM and RT may be essential for determining the radial distribution of the total mixed mass for certain capsules, as well as deciphering measured diagnostic X-ray signatures from *ionized* hot-spot contaminations. To be sure, spallation will cause a higher mass concentration near the pusher surface than where the leading grains stop, but the RM and RT processes may accentuate the increase in mixed mass towards the pusher surface. The resultant radial mixed-mass distribution may be crucial for determining the exact way in which the fuel will burn and hence for predicting ion temperatures, burn width, etc., but *not for predicting capsule yield*, as we can now explain.

M. Crude Burn Theory

We emphasize that the above phenomenology is meant to allow reliable estimation of only a capsule's yield. The fact that the theory does not allow calculation of an exact radial mixed-mass distribution is hence of no consequence here because a capsule's yield depends almost entirely on just the size of the mixed region and not on the radial distribution of spalled mass---as we can now explain. We first note that a capsule's compression does not alter the basic overall configuration of the mixed and clean fuel regions as they were established at the time of grain stoppage. In particular, once the grains stop and diffusion towards an atomically mixed state is underway, as well as subsequent RM and RT instabilities, the demarcation between the clean inner fuel and the contaminated outer fuel generally does not change. More specifically, there is

little tendency for the contaminated material to expand into the clean fuel because the influx of contaminants into the mixed region preserves approximate pressure equilibrium with the clean fuel. Pressure equilibrium is preserved because, although the total material density is increased in proportion to the radial distribution and increased overall by at least a factor of 2, there is a corresponding decrease in temperature due to the added specific heat of the spalled grains. The mixed layer thus has a higher density, but a lower temperature, with its pressure approximately the same as the pressure in the clean fuel.

Because the relative size of the contaminated region does not change once set by the stoppage of the leading spalled grains, capsule yield can be predicted by determining where the leading grains stop—then considering some modifications if the pusher is low Z, because the burn rate is different for chunk and atomic mix in such pushers (but not for high-Z spalled grains). So, for low Z pushers, we must know the diffusive state of the spalled material in the contaminated region, which can vary with radius. We here assume that only the outer contaminated fuel burn efficiency is the one significantly affected and hence degraded by a factor Ψ. Because of the exponential processes involved, we assume

$$\Psi = a\, exp\left[-b\, x_{Diffusion}\right] \qquad 0 < \Psi < 1 \tag{52}$$

where a and b are fitted parameters, perhaps of order 5. Consequently,

$$\frac{Yield_{Predicted}}{Yield_{Clean}} \approx \Psi + \left(1-\Psi\right)\left[1-\frac{\rho_{DT}\Delta r}{\rho_{DT} r_0}\right]^3 \tag{53}$$

where $\rho_{DT}\Delta r$ is the column density of the mixed region via Eq. (25), $\rho_{DT} r_0$ is the total column density of the fuel in its original uncompressed state, and Ψ is the factor by which the outer fuel burn efficiency is suppressed due to the presence of the mix (i.e., the ratio of the burn efficiency with mix to the burn efficiency if there were no mix). In particular, if Ψ is 0 (i.e., the mix completely quenches the burn, as for low or medium Z grains with complete atomic mix), then

$$\frac{Yield_{Predicted}}{Yield_{Clean}} \approx \left[1-\frac{\rho_{DT}\Delta r}{\rho_{DT} r_0}\right]^3 \tag{54}$$

N. How To Use the Model To Estimate a Particular Capsule's Performance

The above model may be used to estimate the performance of a particular capsule by assuming that the DT is in some form of gaseous (or ionized) state as calculated in current hydrodynamics codes, and by using successive runs of these codes intermixed with post-processor-type computer runs that incorporate the drag theory and other effects. This is the way we included the model details to obtain the results presented in Fig. 3 in the main text. Hence, lacking more sophisticated approaches, one may use the following procedure:

1. Make a "clean" 1D run of the capsule using a hydrodynamics/burn code (with the appropriate X-ray drive, etc. but with burn off) up to the time the first shock crosses the pusher-DT interface and establishes a temperature in the DT.
2. Double the initial jump-off velocity of the pusher-DT interface to get v_0.
3. Obtain T_{keV} as the no-burn temperature of the shocked DT.
4. Calculate the initial Reynolds number from Eqs. 21 and 22.

5. Determine the appropriate $\rho_{sp}L_{sp}$ for this pusher (cf. Eq. 4).
6. Calculate the "leading trajectory" of the spalled-material via Eqs. 23 and 24.
7. Use a post-processor code to plot the leading trajectory and the radius-time histories of all DT zones, and determine t_{STOP} as the time the leading trajectory is crossed by the first shock. (We may define the first shock as the locus of points at which the radius-time curves first deviate from their original values.)
8. Decide whether "grain" diffusion is an issue. If the pusher is high Z, skip to step 9. Otherwise, calculate the diffusion time constant via Eq. 47 using the temperature at t_{STOP} as T_{STOP}. Then calculate $x_{Diffusion}$ from Eq. 50 using an appropriate computer program. If $x_{Diffusion} << 1$, then burn will occur in the presence of a chunk mix. For a low-Z pusher, use the hydro/burn code as indicated below. For medium-Z pushers, the chunk mix will modify the burn somewhat, and further hydro/burn code runs must establish the effective burn efficiency (perhaps using Eq. 53).
9. Determine the appropriate radial distribution of mixed mass considering all yield-degradation mechanisms (primarily the spallation, but also RT, RM, fill-tube effects, etc. as appropriate).
10. Re-run the hydro/burn code with burn turned on, imposing the radial distribution of mixed mass as an atomic mix as a function of time up to time t_{STOP} (with the contaminated fuel region set by the leading trajectory).
11. If the pusher is highZ or $x_{Diffusion} >> 1$, just continue the atomically mixed code run to get the capsule's performance.
12. If the pusher is low Z and $x_{Diffusion}$ is of order unity, then an accurate diffusion treatment is required (e.g., run the hydro/burn code in step 10 including the mix in each zone according to its temperature and density history).
13. Run steps 11 or 12 to completion to determine the capsule's performance, with the inner fuel "clean" and the outer fuel contaminated.

Appendix A References

A1. E.g., H. Kolsky, Stress Waves in Solids (N.Y.: Dover Publications, Inc. 1963), p. 181.
A2. R. Lelevier (B. Ragent, ed.), "Lectures on Hydrodynamics and Shock Waves," LLNL Report UCRL-4333 Rev. 1 (Sept. 17, 1965), p. 38.
A3. Ibid., p. 39.
A4. S. F. Hoerner, Fluid-Dynamic Drag: Practical Information on Aerodynamic Drag and Hydrodynamic Resistance (Published by the author, 1965), pp. 3-8, 18-15, 18-22, etc.
A5. Lyman Spitzer, Jr., Physics of Fully Ionized Gases (N.Y.: Interscience Publishers, 1962), p. 146, Eq. (5-54).

This work (LLNL-TR-665701) was performed under the auspices of the U.S. Department of Energy by Lawrence Livermore National Laboratory under Contract DE-AC52-07NA27344.